Petroleum 9 (2023) 214–222

Contents lists available at ScienceDirect

Petroleum

journal homepage: www.keaipublishing.com/en/journals/petlm

Flow characteristic of polymer solutions in porous media: Influence of the molecular weight and concentration

Yingjie Dai [a, b], Jia Li [c], Li Li [d], Yifei Liu [a, b, **], Yuan Li [e], Xiangyu Wang [a, b], Xuguang Song [f], Caili Dai [a, b, *], Bin Yuan [a, ***]

[a] Key Laboratory of Unconventional Oil & Gas Development (China University of Petroleum, East China), Ministry of Education, Qingdao 266580, China
[b] Shandong Key Laboratory of Oilfield Chemistry (China University of Petroleum, East China), Qingdao 266580, China
[c] Nanchong Vocational and Technical College, Nanchong 637131, China
[d] Oil & Gas Technology Research Institute of Changqing Oilfield Company, Xi'an 710000, China
[e] Sinopec Research Institute of Petroleum Engineering, Fracturing & Acidizing and Natural Gas Production Research Institute, Dongying 257000, China
[f] Department of Chemical and Materials Engineering, University of Alberta, Edmonton, AB T6G 1H9, Canada

ARTICLE INFO

Article history:
Received 29 August 2022
Received in revised form
5 November 2022
Accepted 25 March 2023

Keywords:
Polymer solution
Porous media
Flow pattern
μ-PIV

ABSTRACT

The polymer solution flow in porous media is a central research topic related to hydraulic fracturing measures, formation damage and fracture propagation. Influenced by molecular weights and concentrations, various flow patterns of polymer in pores are presented, resulting in different filtration loss. In this work, the effectiveness of various polymer solutions for filtration loss was assessed by utilizing the core flooding experiment firstly. The result shows that lesser filtration loss normally is inextricably linked to solutions with high molecular weight and concentration. Subsequently, the flow behaviors of polymer solutions investigated by designed micro pore-throat structure and micro-particle image velocimetry (μ-PIV) further confirmed the above result. It was found that the central convergent flow pattern benefiting from higher viscous force loss and less filtration loss was observed at high flow rates (0.5 mL/h), and higher molecular weight and concentration were more prone to convergent flow patterns. The viscosity force loss increases by about 4 times varying the molecular weight of polymer from 5×10^6 to 18×10^6 g/mol or the concentration from 0.05 to 0.3%. It interprets higher molecular weight and concentration in core studies and field observations with decreased filtration loss of HPAM. This work provides a theoretical foundation for the application of fracturing fluids as well as fresh perspectives on how to access the filtration loss of fracturing fluids.

1. Introduction

With economic development, the requirement for petroleum has increased rapidly in the past few years [1–3]. Unconventional oil and gas resources are abundant, such as tight oil and gas shale oil and gas [4,5]. However, because of the small matrix and considerable seepage resistance, exploitation of unconventional oil and gas resources requires artificial fracture measures to achieve economic oil and gas flow [2]. Compared to the reserves, unconventional oil and gas resource production is negligible [6]. Hydraulic fracturing technology has proven effective for enhancing oil recovery [7–9], and fracturing fluids are crucial for determining the fracturing effect [10–12]. The flow properties of fracturing fluids in the porous medium of the reservoir can influence the filtration and flow back of fracturing fluid and oil-water displacement [13,14]. Exploring the flow characteristics of fracturing fluid is a long-term question.

Core flooding is a common physical simulation method for studying porous media flow [15,16]. Deghanpour [17] utilized core experiments to investigate how filtration is impacted by the rheological characteristics of viscoelastic fluids. The results demonstrated that the polymer solution's increased elastic

* Corresponding author.
** Corresponding author.
*** Corresponding author.
E-mail addresses: liuyifei@upc.edu.cn (Y. Liu), daicl@upc.edu.cn (C. Dai), yuanbin@upc.edu.cn (B. Yuan).

Peer review under responsibility of Southwest Petroleum University.

Production and Hosting by Elsevier on behalf of KeAi

https://doi.org/10.1016/j.petlm.2023.03.002

characteristics decreased filtration loss. Despite this approach can nevertheless acquire macroscopic results like pressure drop and oil output, the flow properties in the pore structure are not measurable. The recent development of microfluidic devices introduces a novel idea for directly studying fluid flow behaviors in micropore units [18–21]. The velocity field of a viscoelastic fluid has been quantitatively investigated in recent research [22,23]. Jagdale et al. [24] experimentally studied the effect of fluid rheological properties on non-Newtonian flow in microchannels. They summarized each viscoelastic fluid's flow patterns and vortex development in the dimensionless Wi − *Re* and χL − *Re* parameter spaces. In addition, the flow of polyethylene oxide solutions through prepared micropores was investigated by Rodd et al. They demonstrated the mechanism of inertial-elastic flow influenced by PEO concentration [25]. The rheology of polymer influences the flow of polymer in porous media, but the influence mechanism is not clear.

In this work, hydrolyzed polyacrylamide (HPAM) solution, one of the representative hydraulic fracturing fluid systems [26,27], which has the advantages of low formation damage and low cost [28], was used. Filtration tests of the real rock samples by changing molecular weight and concentration of polymer were performed to compare filtration loss of fracturing fluid with different molecular weights and concentrations. Then, a continuous micro-diverging-converging structure is used for microfluidic investigations, where the flow patterns of HPAM solutions are examined and contrasted with those of a Newtonian fluid. The influence mechanism of molecular weight and concentration of polyacrylamide on its flow in porous media further illustrates the results of the filtration model experiment.

2. Materials and methods

2.1. Microchannel design

The specified microfluidic channel was constructed using precision milling on a polymethyl methacrylate (PMMA) plate. Another PMMA plate is secured with a dense screw connected to the designed PMMA plate. An injection point, an outflow point, two pressure measurement points, and two pore units made up a microchannel. (Fig. 1). This design made the experimental fluid stable when it reached the pore units. Upstream and downstream of the pore unit were contraction-expansion and expansion-contraction structures, respectively. To get accurate flow rates from 0.05 ml/h to 10 ml/h, the solution at the intake was connected to a Hamilton syringe and the syringe was propelled by a Harvard pump.

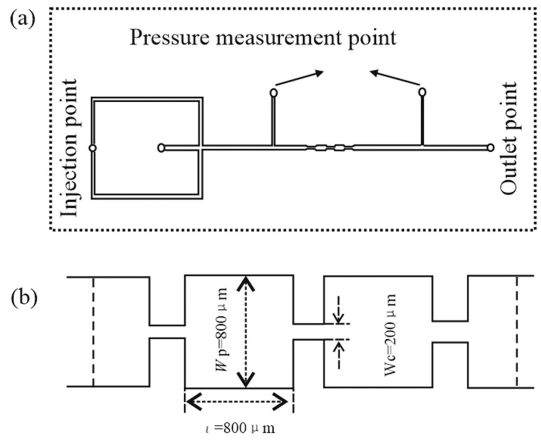

Fig. 1. Design of the microchannels (a) and (b).

2.2. Fluid rheological characteristics

Polymer solution with various molecular weights was prepared in our investigation, while a Newtonian solution served as the contrast. Hydrolyzed polyacrylamide (HPAM) with molecular weights of 5×10^6 g/mol, 8×10^6 g/mol, and 18×10^6 g/mol was used as the main agent of viscoelasticity fluid. The 55 wt% glycerol water solution was employed as the control group fluid with a viscosity of 6 mPa·s. The viscosity of the selected glycerol-aqueous solution system was similar to that of the polymer solution at 170 s^{-1} shear rate. The rheological properties (Steady shear viscosity, Viscoelastic modulus) were measured using HAAKE MARS 60 Rheometer.

2.3. Dimensionless parameters

The Reynolds number (*Re*) is the similarity criterion number to characterize the viscous effect in fluid mechanics [29]. The definition of Reynolds number (*Re*) is:

$$Re = \frac{\rho \overline{V_p} D_h}{\eta_p} = \frac{2\rho Q}{(W_p + h)\eta_p} \tag{1}$$

Here, the hydraulic diameter $D_h = \frac{2W_p h}{W_p + h}$.

The Deborah number (De) is the ratio of a solution's relaxation time to the flow's detention duration [30]. The definition of Deborah number (*De*) is:

$$De = \frac{\lambda_1}{w_p l h / Q} = \frac{\lambda_1 Q}{w_p l h} \tag{2}$$

Each parameter unit and its physical meaning are listed in Table 1.

2.4. Filtration experimental design

The core data used in the four groups of experiments were shown in Table 2. The cores were initially soaked for 24 h with simulated formation water (Parameters are listed in Table 3). Fig. 2 showed the flowchart for the filtration loss experiment. The stainless steel tubing was filled with simulated formation water, and the core was put into the core holder. Then, the injection pressure was kept at 3.8 MPa while 9 MPa was chosen as the core holder's confining pressure. The first droplet that entered the measuring cylinder marked the commencement of filtration starting. Different time points (1, 4, 9, 16, 25, and 36 min) and related filtration volumes were recorded in order to calculate filtration loss.

Table 1
Parameter list.

Parameter	Physical meaning
W_c (μm)	Width of the channel
W_p (μm)	Width of the pore
Re	Reynolds number
De	Deborah number
ρ (g/cm^3)	Solution density
D_h (μm)	Hydraulic diameter
η_p (mPa·s)	Shear-viscosity
$\overline{V_p}$ (m/s)	Average flow velocity in a pore channel
h (μm)	Hight of the channel
λ_1 (s)	Relaxation time
G' (Pa)	Storage modulus
G" (Pa)	Loss modulus

Table 2
Core property.

Core No.	Fluid	Length (mm)	Diameter (mm)	Porosity (%)	Permeability (mD)	Saturation (%)
1	HPAM 1	49.02	25.50	18.04	14.3	85.32
2	HPAM 2	49.40	25.50	17.41	14.3	85.57
3	HPAM 3	48.24	25.30	18.56	14	86.51
4	Newtonian fluid	50.00	25.30	24.41	14	80.35

Notes：HPAM 1 - Concentration is 0.05 wt% and molecular weight is 8×10^6 g/mol.
HPAM 2 - Concentration is 0.05 wt% and molecular weight is 18×10^6 g/mol.
HPAM 3 - Concentration is 0.3 wt% and molecular weight is 8×10^6 g/mol.
Newtonian fluid - Glycerol aqueous solution with a concentration of 55 wt%.

Table 3
Parameters of simulated formation water.

Composition	Ca^{2+}	Mg^{2+}	Na^{+}	K^{+}	Cl^{-}	Total
Concentration ($mg \cdot L^{-1}$)	1985.95	1136.84	21646.13	10489.60	49745.16	85003.69

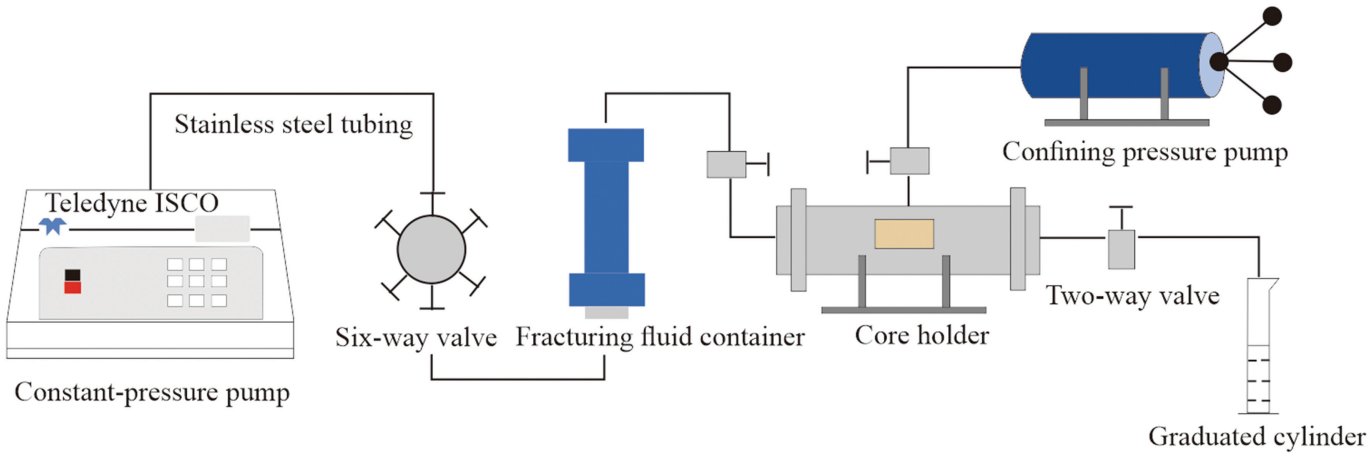

Fig. 2. Flow chart of filtration performance evaluation experiment.

2.5. Flow pattern determination method

Microparticle image velocimetry was served to quantitatively measure the flow field in the pore structure. Fluorescent particles mainly composed of polystyrene were blended into the experimental fluids. The laser illuminates the fluorescent particles, and the high-speed camera exposes the moving position of the fluorescent particles twice. The computer calculated the instantaneous velocity of particles in the whole field. The delay time (dt) between selected laser pulse pairs depended on the efficient movement of illumination particles about 8 pixels, enabling more precise calculation. The motion vector diagram of the fluorescent particles could be transformed into the flow field of the whole fluid in the region because the fluorescent particles were flowing with the fluid.

3. Result and discussion

3.1. Filtration loss of Newtonian fluid and HPAM solution

The rheology measurement result (Steady shear viscosity, Viscoelastic modulus) was shown in Fig. 3. The relaxation time λ_1 was defined as the reciprocal of the intersection frequency of loss modulus and storage modulus [31]. And it referred to the time required for polymer molecules to change from a non-equilibrium state to an equilibrium state. According to Fig. 3(b), the relaxation times can be obtained, are 2.22, 1.20, and 0.88 s in turn.

The calculation formula of experimental filtration coefficient (C) was as follows:

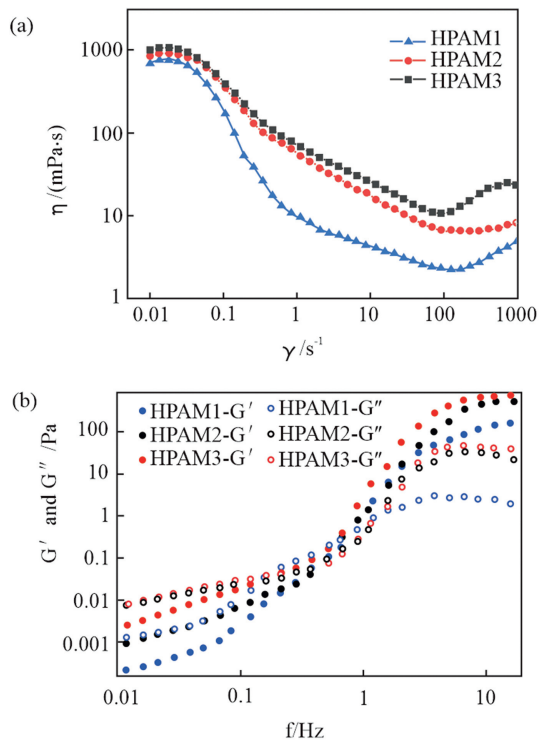

Fig. 3. (a) Shear viscosity curve of the HPAM solutions (b) Curve of viscoelastic modulus test.

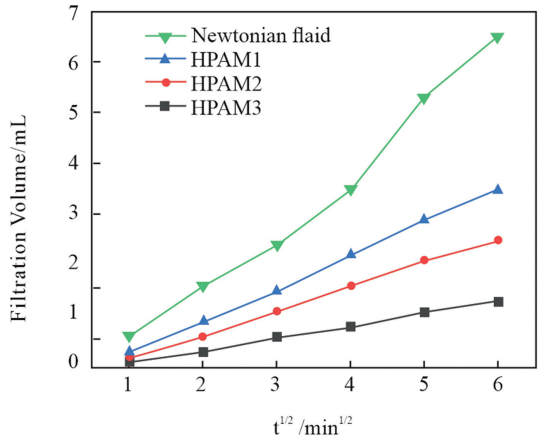

Fig. 4. Filtration curves of the different solutions.

$$C = 0.005 \times m/A \quad (3)$$

where, C is the filtration coefficient of fracturing fluid, m/min$^{1/2}$; m is the slope of the filtration curve, ml/min$^{1/2}$; A is the acreage of the core, cm^2 [32].

The cores used for the core displacement experiment had similar properties (porosity, permeability, and saturation). The slopes of the filtration loss curves are 1.19, 0.65, 0.47, and 0.25 ml/min$^{1/2}$, respectively, as illustrated in Fig. 4. The filtration coefficient is 6.07 × 10^{-4} m/min$^{1/2}$ for the Newtonian fluid for the cores with the permeability of 14 μm^2, and 3.32 × 10^{-4}, 2.40 × 10^{-4}, and 1.28 × 10^{-4} m/min$^{1/2}$ for HPAM1, HPAM2, and HPAM3 for the cores with similar permeability. The filtration coefficient C of these two types of fluids differ even though their viscosities are the same at shear speeds of 170 s^{-1}. Different fracturing fluids' filtering abilities cannot be adequately assessed by viscosity. Performance of

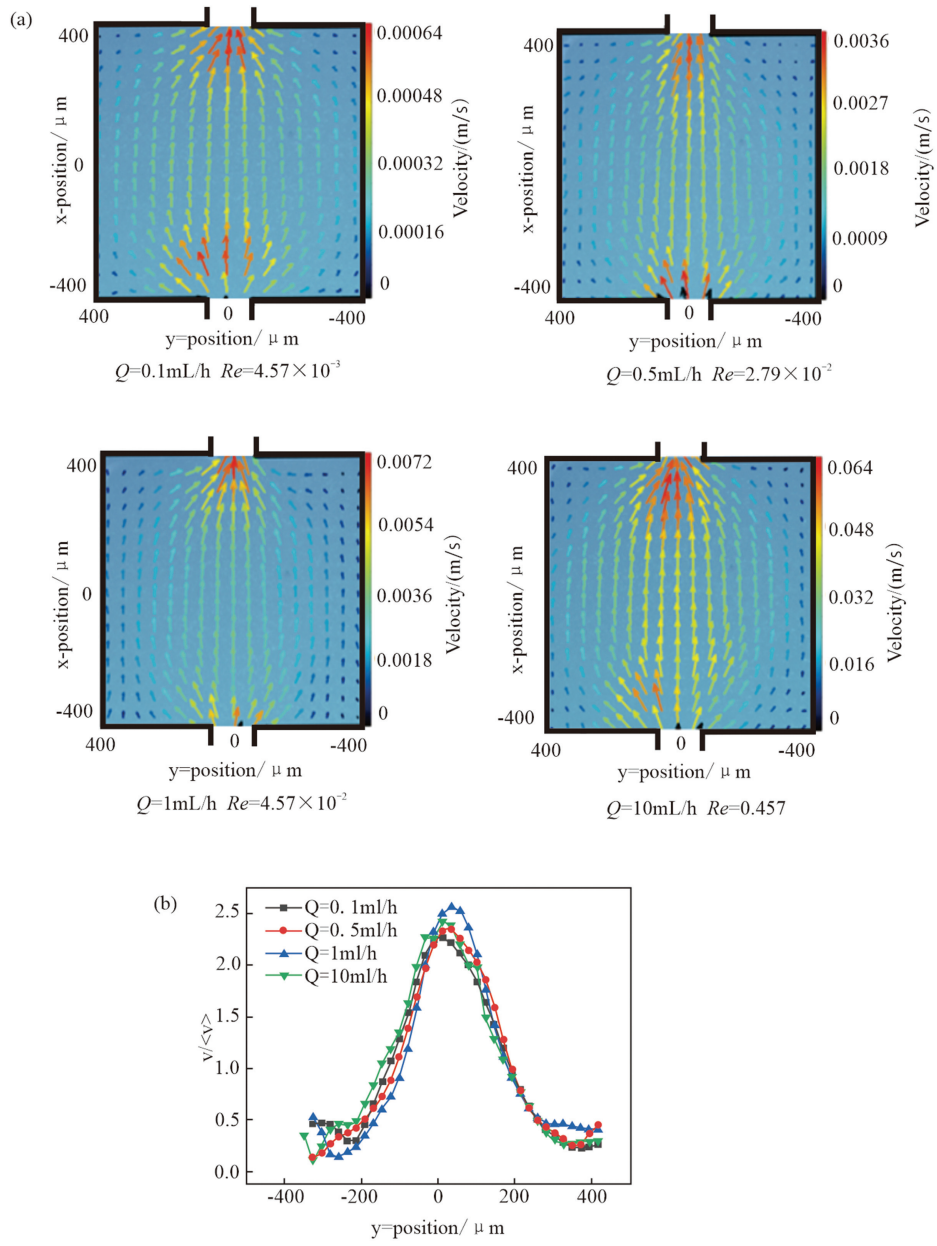

Fig. 5. (a) Flow patterns images of the glycerol-water solution in the pore structure. (b) Curve of velocity in y direction at x = −200 μm.

filtration is also significantly influenced by elastic properties and pore unit flow patterns.

3.2. Flow pattern of HPAM solutions

3.2.1. Flow pattern of Newtonian fluid

The velocity field of the glycerol-water solution (one type of Newtonian fluid) in the designed pore structure was shown in Fig. 5. Newtonian fluid had the same flow patterns with the increase in flow rates. The change of injection flow rates only affected the maximum velocity of the Newtonian fluid in the pore structure. Glycerol aqueous solution only had two kinds of small molecules merely, glycerol and water, and its viscosity would not change with shear rate. The dimensionless velocity components in the Y direction were in close proximity to one another with an increase in *Re* from 4.57×10^{-3} to 0.457.

The flow pattern of Newtonian fluid was as follows: The velocity was composed of the velocity components in the x-axis and Y-axis direction at the joint of the channel and throat. With the development of flow, the velocity at the middle part of the throat decreased gradually, and the flow velocity was mainly in the x-axis direction and had little change. Then the streamline gradually converged from both sides to the centerline, and the center velocity increased and the velocity decreased on both sides. Finally, the maximum flow velocity was reached at the junction of the channel and throat. The alteration in the glycerol aqueous solution's flow pattern accorded with the explanation of classical hydrodynamics.

3.2.2. Effect of polymer molecular weight

Fig. 6 illustrated the velocity field of HPAM solution with different polymer molecular weights (5×10^6 g/mol, 18×10^6 g/mol) in the pore structure. Low flow rate velocity fields resembled the velocity field of the Newtonian fluid. The streamline was divergent upstream of the pore structure and then gradually shrank down to the centerline downstream. The velocity field of HPAM solutions and that of Newtonian fluid, however, differed in some aspects. The streamline of the HPAM solution shrank to the centerline earlier downstream. The velocity field of the HPAM solution altered differently from the Newtonian fluid with an increase in injection flow rates. The flow pattern of HPAM maintained the center convergence from intake to outlet when the injection velocity was larger than 1 mL/h.

Additionally, no velocity component exists in the y-direction, just along the x-axis. The velocity along the centerline was relatively high compared to that away from the centerline. The long-chain molecules of the polymer were unable to be fully stretched in the direction vertical to the flow direction when the polymer solution converged to the divergent-shrink structure at a high flow rate, leading to no discernible expansion of the streamline. That is to say, the classical viscoelastic fluid naturally tended to maintain the original flow patterns.

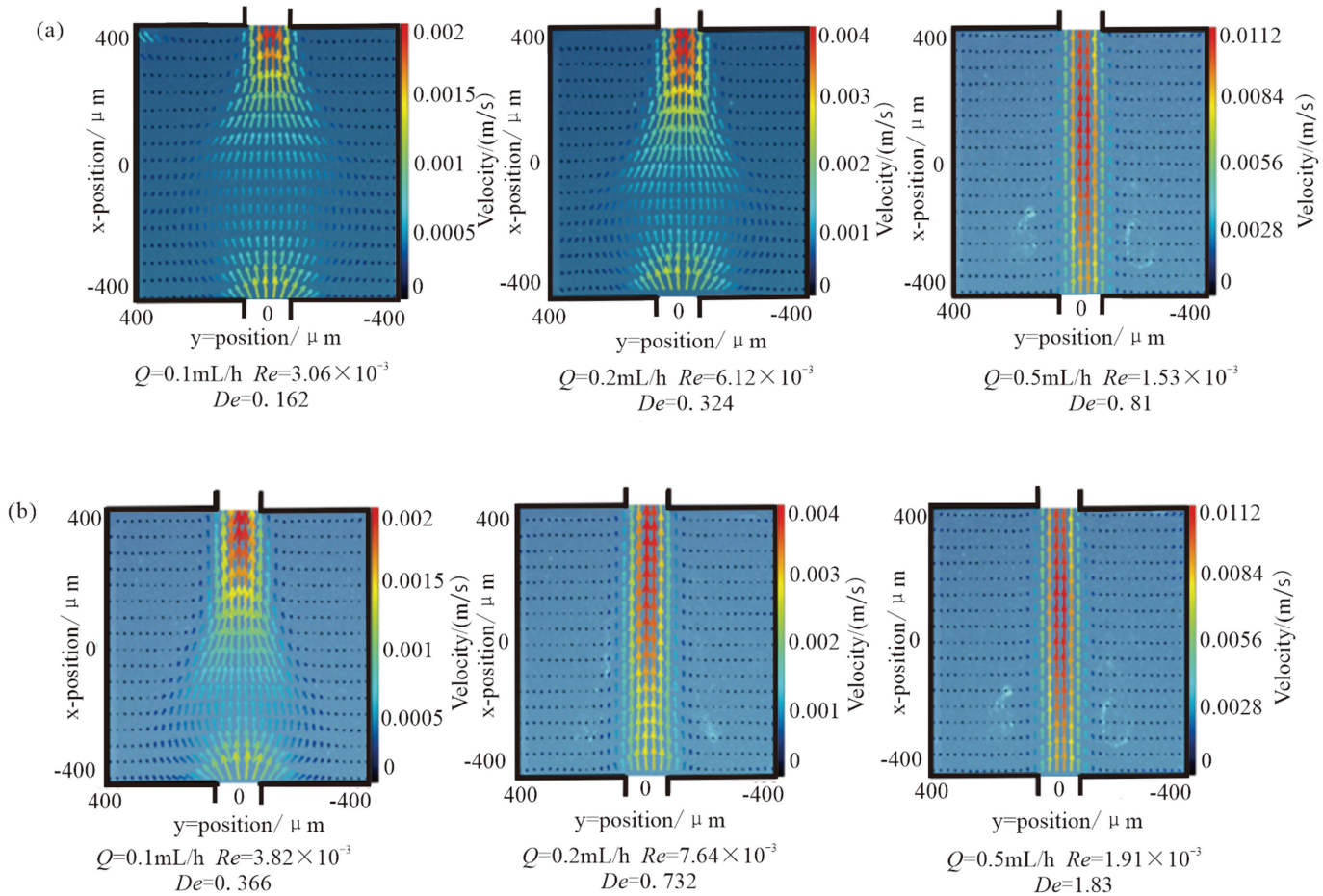

Fig. 6. (a) Flow patterns images of the polymer solution with a molecular weight of 500×10^6 g/mol in the pore structure. (b) Flow patterns images of the polymer solution with a molecular weight of 18×10^6 g/mol.

The change of velocity field of HPAM with different molecular weights was similar, but there were still differences. It could be seen from the previous paragraph that the flow pattern of HPAM solutions would change from divergent to central convergent after reaching a critical flow rate. The flow pattern of HPAM solution with a molecular weight of 18 × 10^6 g/mol changed from divergent to central convergence at a lower flow rate (Q = 0.2 mL/h), while the HPAM solution with a molecular weight of 5 × 10^6 g/mol changed at Q = 0.5 mL/h. The larger the molecular weight of the polymer was, the longer the molecular chain segment was, polymer molecule was easier to form a coil. It was more inclined to maintain the original flow state when passing through the pore throat. Therefore, the critical velocity of flow regime transition of the high molecular weight polymer solution was lower.

3.2.3. Effect of polymer concentration

The velocity fields of HPAM solutions with different polymer concentrations (0.05 wt%, 0.3 wt%) in the pore unit were tested in this study. The HPAM flow pattern change as the polymer molecular weight increased in Fig. 7 was comparable to the HPAM flow pattern change as the polymer concentration increased in Fig. 5. With the increase of flow rates (Q) from 0.1 mL/h to 0.5 mL/h, the *Re* increases by 4 times. The flow of the HPAM solutions in the pore structure was steady laminar flow with *Re* under 2000. However, similar to the effect of polymer molecular weight, the flow pattern of HPAM solution changed from divergent to central convergent. The width of the flow pattern was stable and slightly wider than the pore throat. Also, the higher the polymer concentration was, the lower velocity of flow pattern transition was.

3.3. Velocity profile in pore unit

3.3.1. Comparison of polymer solutions with different molecular weight

To demonstrate the velocity variation between the solutions with various molecular weights at the same x-direction (x = 200 μm), three flow rate settings were chosen to obtain flow field data in the pore structure, as shown in Fig. 8. The x-direction was chosen to make it easier to find differences in the flow fields of different systems.

The velocity profiles are broadly unchanged for the Newtonian fluid (black lines in Fig. 8) with varying flow rates, showing a parabolic distribution. There is almost a velocity distribution in the y-direction (y = −400 to 400 μm). Moreover, the maximum velocity was more significant than the minimum velocity. Visually, the velocity distribution is relatively uniform.

The velocity distribution of HPAM solutions (red and blue lines in Fig. 8) exhibited a single-peak state, essentially remaining unchanged when the flow rate is more than 1 ml/h. In addition, the majority of the velocity was dispersed in a fixed zone (y = -100 to 100 μm), and the center velocity line was where the highest velocity was concentrated. The velocity distribution was quite

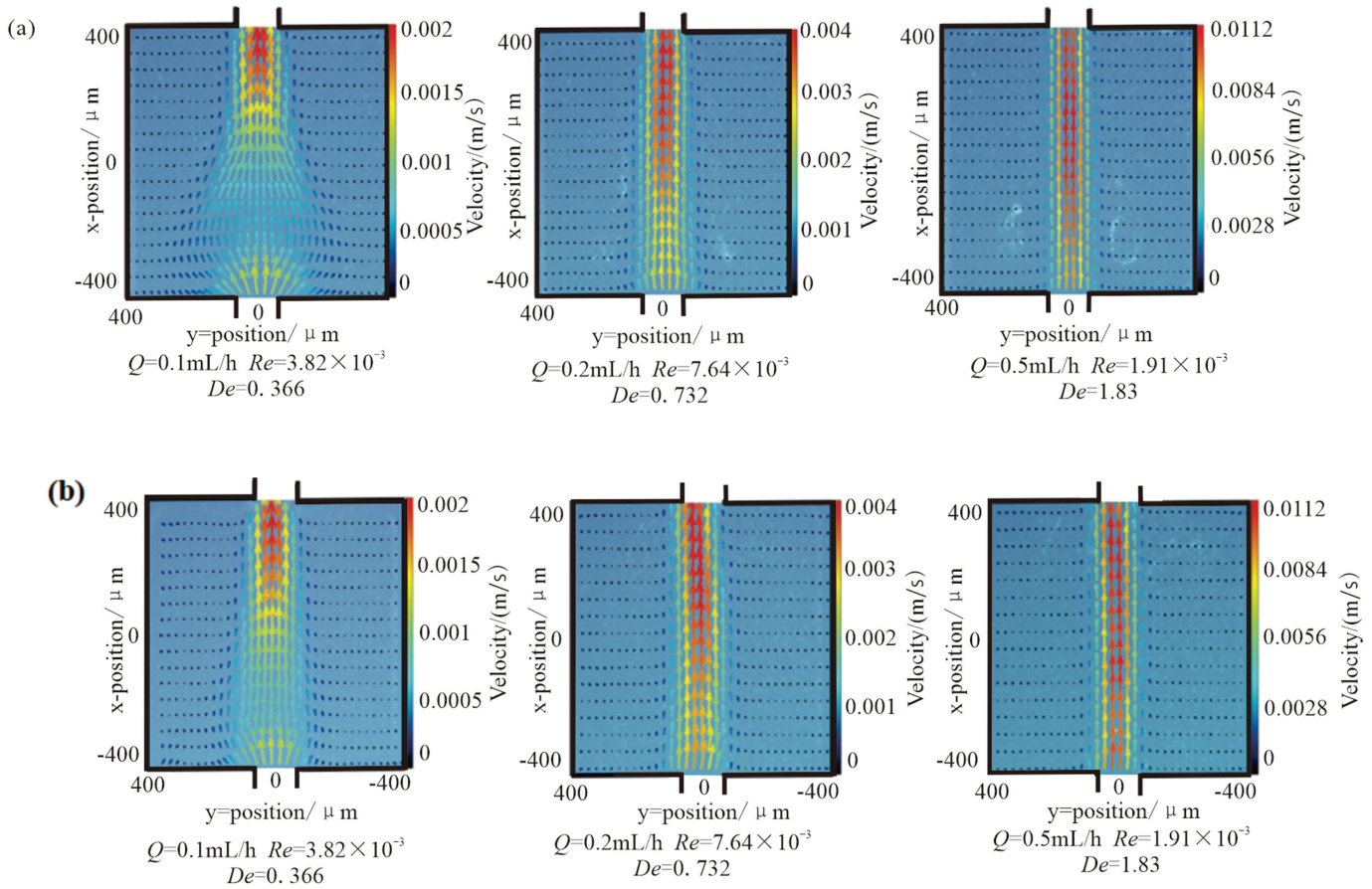

Fig. 7. (a) Flow patterns images of the polymer solution with a concentration of 0.05 wt% in the pore structure. (b) Flow patterns images of the polymer solution with a concentration of 0.3 wt%.

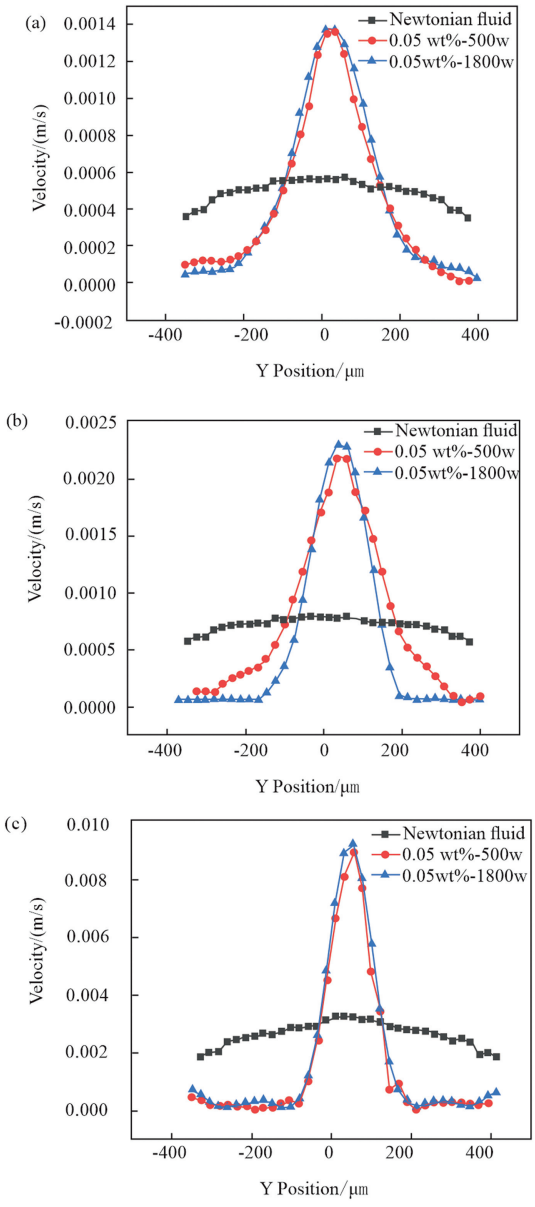

Fig. 8. Curve of velocity distribution in y direction of the solutions flowing through the pore structure (x = 200 μm) at flow rates (a) Q = 0.1 ml/h, (b) Q = 0.2 ml/h, (c) Q = 0.5 ml/h.

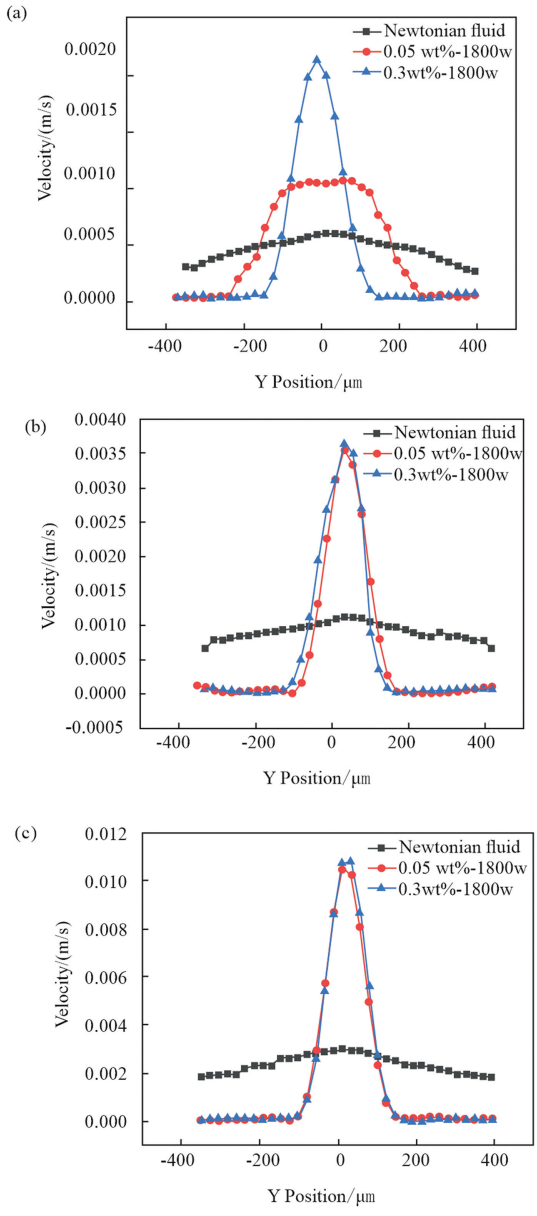

Fig. 9. Curve of velocity distribution in y direction of the solutions flowing through the pore structure (x = 0 μm) at flow rates (a) Q = 0.1 ml/h, (b) Q = 0.2 ml/h, (c) Q = 0.5 ml/h.

extensive when the flow rate was smaller than 1 mL/h. The velocity distribution of HPAM solution with molecular weight of 5×10^6 g/mol is from y = −200 μm to y = 200 μm when Q = 0.1 ml/h. The HPAM solution with a molecular weight of 18×10^6 g/mol has the same characteristics as the above solution. However, the velocity distribution of HPAM solution with molecular weight of 18×10^6 g/mol shrunk significantly (y = −100 to 100 μm) different from the 5×10^6 g/mol when Q = 0.2 mL/h. According to Newton's law of internal friction, viscous force loss of the HPAM solution with a molecular weight of 18×10^6 g/mol is nearly 4 times greater than that of the 5×10^6 g/mol.

In summary, the velocity profile is the quantification of the flow pattern. The critical velocity for the contraction of the velocity distribution of the HPAM solution with high molecular weight is smaller, in addition, greater viscous force loss will be produced when the HPAM solution passes through the pore unit.

3.3.2. *Comparison of polymer solutions with different concentration*

Fig. 9 showed the velocity profile of the HPAM solutions with different concentrations at x = 0 μm. The velocity profile of Newtonian fluid at x = 0 μm kept a good resemblance with the area at x = 200 μm. No apparent velocity aggregation is found. As *Re* increased further, the velocity profiles of HPAM solutions with different concentrations were similar, remaining single-peak shape. The overall trend observed in Fig. 9 is that the speed line

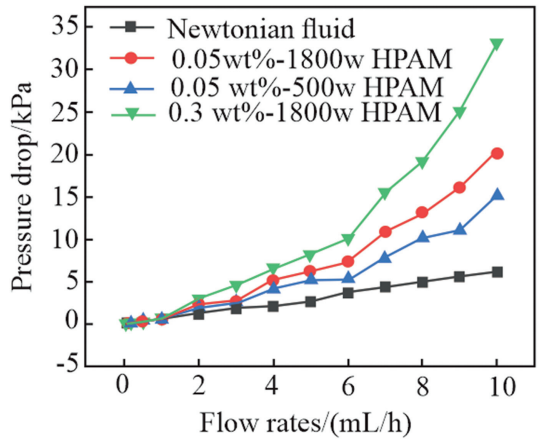

Fig. 10. Pressure drop test chart of different systems.

of the HPAM solution with a higher concentration (0.3 wt%) shrunk at a lower value of *Re*. Moreover, the loss of viscous force increased by 4.85 times with the solution concentration increased by 0.25 wt %, which was conducive to the hydraulic fracturing operation.

3.4. Pressure drop in pore structure

The pressure drop of two pressure measuring points caused by each solution through the channel was measured individually, and its correlation with flow rate was studied. Fig. 10 demonstrated that the pressure drop of each system was not noticeably different when the flow rate was less than 1 ml/h, and the flow pattern of the polymer solutions was comparable to that of Newtonian fluid under the same conditions. The Newtonian fluid pressure drop and flow rate exhibited a linear connection, with a constant slope of 0.62 in accord with the Darcy seepage law. The slope of polymer curve changed obviously when the flow rate exceeded 1 ml/h. Under the identical circumstances, the polymer flow pattern shifted from divergent to central convergent.

For all flow patterns, the flow velocity close to the inlet and outlet of the microchannel increased significantly and the streamline was obviously concentrated, because of the change of flow section area. Polymer solutions had distinctive viscoelasticity in comparison to Newtonian fluid, which lead to the additional pressure drop. As a result, contraction flows formed by polymer systems farther from microchannel exits were made easier. The flow patterns of polymer solutions in the pore structure displayed a sever contraction and the flow line was limited to a rectangular area from the entrance to the exit. The polymer system passed through the pore structure at a high flow rate, with almost no velocity component perpendicular to the flow direction, making it easier to pass through and resulting in lower filtration loss.

4. Conclusion

In this study, rheological experiment, filtration performance evaluation experiment, microfluidic experiment and pressure drop test were conducted in this work to investigate the difference between the flow characteristics of polymer solution and Newtonian fluid, as well as the influence mechanism of molecular weight and concentration on the flow properties of polymer solution in porous media.

Based on the findings of the above experiments, Based on the findings of the above experiments, the following conclusions were reached.

(1) Filtration losses of HPAM solutions are lower than that of Newtonian fluid, even though they might share similar shear viscosities at the same shear rates. It might not be accurate to anticipate filtration loss solely based on viscosity data.
(2) The HPAM solution's flow patterns were considerably different from those of Newtonian fluid. The flow pattern of Newtonian fluid stays divergent all time. The streamline of HPAM solution was divergent under low shear rates. However, the streamline maintained the contraction from inlet to outlet when a critical flow rate was reached.
(3) Increasing the molecular weight or concentration of HPAM solution causes the enhancement of molecular network structure strength, reduction of relaxation time, and the critical flow velocity for flow pattern transition. The pressure drop between the inlet and outlet is obviously increased, contributing to the lower filtration losses.

In addition, this study offers a straightforward and affordable measure to assess the filtration capabilities of various fracturing solutions. It can be used as a useful addition to traditionally expensive core tests.

Acknowledgements

The authors appreciate the support from National Key Research and Development Program of China (NO. 2022YFE0129900). The authors desire to thank one of the reviewers profusely for offering constructive comments which helped in improving the paper considerably.

References

[1] F.G. Adams, Y. Shachmurove, Modeling and forecasting energy consumption in China: implications for Chinese energy demand and imports in 2020, Energy Econ. 30 (3) (2008) 1263–1278, https://doi.org/10.1016/j.eneco.2007.02.010.
[2] L.A. Patterson, K.E. Konschnik, H. Wiseman, J. Fargione, K.O. Maloney, J. Kiesecker, et al., Unconventional oil and gas spills: risks, mitigation priorities, and state reporting requirements, Environ. Sci. Technol. 51 (5) (2017) 2563–2573, https://doi.org/10.1021/acs.est.6b05749.
[3] L. Tripathi, A.K. Mishra, A.K. Dubey, C.B. Tripathi, P. Baredar, Renewable energy: an overview on its contribution in current energy scenario of India, Renew. Sustain. Energy Rev. 60 (2016) 226–233, https://doi.org/10.1016/j.rser.2016.01.047.
[4] Z. Caineng, Y. Zhi, Z. Rukai, Z. Guosheng, H. Lianhua, W. Songtao, et al., Progress in China's unconventional oil & gas exploration and development and theoretical technologies, Acta Geologica Sinica - English Edition 89 (3) (2015) 938–971, https://doi.org/10.1111/1755-6724.12491.
[5] H. Wang, F. Ma, X. Tong, Z. Liu, X. Zhang, Z. Wu, et al., Assessment of global unconventional oil and gas resources, Petrol. Explor. Dev. 43 (6) (2016) 925–940, https://doi.org/10.1016/S1876-3804(16)30111-2.
[6] L. Zheng, P. Wei, Z. Zhang, S. Nie, X. Lou, K. Cui, et al., Joint exploration and development: a self-salvation road to sustainable development of unconventional oil and gas resources, Nat. Gas. Ind. B 4 (6) (2017) 477–490, https://doi.org/10.1016/j.ngib.2017.09.010.
[7] J. Liu, J.J. Sheng, H. Emadibaladehi, J. Tu, Experimental study of the stimulating mechanism of shut-in after hydraulic fracturing in unconventional oil reservoirs, Fuel 300 (2021) 120982, https://doi.org/10.1016/j.fuel.2021.120982.
[8] Z. Liu, Z. Pan, S. Li, L. Zhang, F. Wang, L. Han, et al., Study on the effect of cemented natural fractures on hydraulic fracture propagation in volcanic reservoirs, Energy 241 (2022) 122845, https://doi.org/10.1016/j.energy.2021.122845.
[9] I. Pană, I.V. Gheţiu, I.G. Stan, F. Dinu, G. Brănoiu, S. Suditu, The use of hydraulic fracturing in stimulation of the oil and gas wells in Romania, Sustainability 14 (9) (2022), https://doi.org/10.3390/su14095614.

[10] A.C. Barbati, J. Desroches, A. Robisson, G.H. McKinley, Complex fluids and hydraulic fracturing, Annu. Rev. Chem. Biomol. Eng. 7 (1) (2016) 415–453.
[11] B. Wang, B. Liu, J. Yang, L. Bai, S. Li, Compatibility characteristics of fracturing fluid and shale oil reservoir: a case study of the first member of Qingshankou Formation, northern Songliao Basin, Northeast China, J. Petrol. Sci. Eng. 211 (2022) 110161, https://doi.org/10.1016/j.petrol.2022.110161.
[12] J. Wang, D. Elsworth, Y. Wu, J. Liu, W. Zhu, Y. Liu, The influence of fracturing fluids on fracturing processes: a comparison between water, oil and SC-CO2, Rock Mech. Rock Eng. 51 (1) (2018) 299–313.
[13] C. Dai, Y. Li, Q. Xie, K. Xu, Y. Hu, Z. Zhou, et al., Reduction of clean fracturing fluid filtration loss by viscosity enhancement using nanoparticles: is it feasible? Chem. Eng. Res. Des. 156 (2020) 414–424, https://doi.org/10.1016/j.cherd.2020.02.017Get.
[14] Z. Ge, S. Gong, Z. Zhou, M. Ye, Z. Wang, H. Zhang, et al., Influence of viscoelastic surfactant fracturing fluids on modified coal fracture flow characteristics, Energy & Fuels 36 (3) (2022) 1495–1506, https://doi.org/10.1021/acs.energyfuels.1c03951.
[15] V.A. Mosin, D.N. Voitenko, A.V. Bulgakov, S.V. Vasilchenko, A.V. Medentsev, On the return permeability definition by core flow study as a method for preliminary assessment of drill-in quality (Russian), Neftyanoe khozyaystvo - Oil Industry 2018 (10) (2018) 42–46, https://doi.org/10.24887/0028-2448-2018-10-42-46.
[16] H. Saboorian-Jooybari, M. Dejam, Z. Chen, Heavy oil polymer flooding from laboratory core floods to pilot tests and field applications: half-century studies, J. Petrol. Sci. Eng. 142 (2016) 85–100, https://doi.org/10.1016/j.petrol.2016.01.023.
[17] H. Dehghanpour, E. Kuru, Effect of viscoelasticity on the filtration loss characteristics of aqueous polymer solutions, J. Petrol. Sci. Eng. 76 (1) (2011) 12–20, https://doi.org/10.1016/j.petrol.2010.12.005.
[18] H.-S. Dou, N. Phan-Thien, Viscoelastic flow past a confined cylinder: instability and velocity inflection, Chem. Eng. Sci. 62 (15) (2007) 3909–3929, https://doi.org/10.1016/j.ces.2007.03.040.
[19] K. Ma, R. Liontas, C.A. Conn, G.J. Hirasaki, S.L. Biswal, Visualization of improved sweep with foam in heterogeneous porous media using microfluidics, Soft Matter 8 (41) (2012).
[20] M.K. Mulligan, J.P. Rothstein, The effect of confinement-induced shear on drop deformation and breakup in microfluidic extensional flows, Phys. Fluids 23 (2) (2011), https://doi.org/10.1063/1.3548856.
[21] Y. Wu, R. Wang, C. Dai, Y. Xu, T. Yue, M. Zhao, Precisely tailoring bubble morphology in microchannel by nanoparticles self-assembly, Ind. Eng. Chem. Res. 58 (9) (2019) 3707–3713, https://doi.org/10.1021/acs.iecr.8b06057.
[22] Y. Li, C. Dai, Y. Wu, K. Xu, M. Zhao, Y. Wang, Viscoelastic surfactant fluids filtration in porous media: a pore-scale study, AIChE J. 66 (6) (2020), https://doi.org/10.1002/aic.16229.
[23] Y. Li, R. Wang, R. Wang, W. Liu, C. Dai, X. Yao, et al., Investigation on flow characteristic of viscoelasticity fluids in pore-throat structure, J. Petrol. Sci. Eng. 174 (2019) 821–832, https://doi.org/10.1016/j.petrol.2018.12.003.
[24] P.P. Jagdale, D. Li, X. Shao, J.B. Bostwick, X. Xuan, Fluid rheological effects on the flow of polymer solutions in a contraction–expansion microchannel, Micromachines 11 (3) (2020), https://doi.org/10.3390/mi11030278.
[25] L.E. Rodd, T.P. Scott, D.V. Boger, J.J. Cooper-White, G.H. McKinley, The inertio-elastic planar entry flow of low-viscosity elastic fluids in micro-fabricated geometries, J. Non-Newtonian Fluid Mech. 129 (1) (2005) 1–22.
[26] E. Aliabadian, S. Sadeghi, M. Kamkar, Z. Chen, U. Sundararaj, Rheology of fumed silica nanoparticles/partially hydrolyzed polyacrylamide aqueous solutions under small and large amplitude oscillatory shear deformations, J. Rheol. 62 (5) (2018) 1197–1216, https://doi.org/10.1122/1.5024384.
[27] W.J.R. Gilbert, S.J. Johnson, J.-S. Tsau, J.-T. Liang, A.M. Scurto, Enzymatic degradation of polyacrylamide in aqueous solution with peroxidase and H_2O_2, J. Appl. Polym. Sci. 134 (10) (2017), https://doi.org/10.1002/app.44560.
[28] S. Fakher, M. Ahdaya, A. Imqam, Hydrolyzed polyacrylamide – fly ash reinforced polymer for chemical enhanced oil recovery: Part 1 – injectivity experiments, Fuel 260 (2020) 116310, https://doi.org/10.1016/j.fuel.2019.116310.
[29] D.B. Pitz, A.T. Franco, C.O.R. Negrão, Effect of the Reynolds number on viscoelastic fluid flows through axisymmetric sudden contraction, J. Braz. Soc. Mech. Sci. Eng. 39 (5) (2017) 1709–1720.
[30] J.C. Wu, N.A. Peppas, Modeling of penetrant diffusion in glassy polymers with an integral sorption deborah number, J. Polym. Sci. B Polym. Phys. 31 (11) (1993) 1503–1518, https://doi.org/10.1002/polb.1993.090311108.
[31] J. Zhu, Z. Yang, X. Li, Z. Song, Z. Liu, S. Xie, Settling behavior of the proppants in viscoelastic foams on the bubble scale, J. Petrol. Sci. Eng. 181 (2019) 106216, https://doi.org/10.1016/j.petrol.2019.106216.
[32] H. Tang, H. Tang, J. He, F. Zhao, L. Zhang, J. Liao, et al., Damage mechanism of water-based fracturing fluid to tight sandstone gas reservoirs: improvement of the Evaluation Measurement for Properties of Water-based Fracturing Fluid: SY/T 5107-2016, Nat. Gas. Ind. B 8 (2) (2021) 163–172, https://doi.org/10.1016/j.ngib.2020.09.016.